**Article:**

# The aqueous phase behaviour of a NaLAS-polycarboxylate polymer system

Mariam Hussain,[†] Mamatha Nagaraj,[‡] Olivier J. Cayre,[†] Eric S. J. Robles,[¶] Hossam Tantawy,[§] and Andrew E. Bayly[*,†]

†*School of Chemical and Process Engineering, University of Leeds, Leeds, LS2 9JT.*

‡*School of Physics and Astronomy, University of Leeds, Leeds, LS2 9JT.*

¶*The Procter and Gamble Company, Newcastle Innovation Centre, Newcastle-Upon-Tyne NE12 9TS, United Kingdom.*

§*The Procter and Gamble Company, Newcastle Innovation Centre, Newcastle-Upon-Tyne, NE12 9TS, United Kingdom.*

E-mail: a.e.bayly@leeds.ac.uk

**Abstract**

Linear Alkylbenzene Sulphonate (NaLAS) surfactant is often combined with poly-carboxylate polymers in detergent formulations. However, the behaviour of these aqueous surfactant-polymer systems in the absence of added electrolyte is unreported. This work investigates the behaviour of such systems using polarised-light microscopy, SAXS, centrifugation and $^2$H NMR techniques. A phase diagram at 50°C is reported for 0 to 50 wt% NaLAS concentrations and 0 to 10 wt% polycarboxylate concentrations. The NaLAS-water system is micellar at concentrations < 35 wt%, and a 2-phase micellar-lamellar system is seen at higher NaLAS levels, consistent with what has been reported by previous studies. As polymer is added at low surfactant concentrations (∼10 - 20 wt% NaLAS), a second optically isotropic phase is formed, this is thought to be a

1

polymer-rich phase. Further addition of polycarboxylate leads to the formation of a lamellar phase. At high surfactant concentrations (>20 wt% NaLAS), the addition of polymer induces a second lamellar phase. These observed behaviours are thought to arise as a result of depletion flocculation and salting out effects. The observed lamellar phases adopt colloidal multilamellar vesicle (MLV) structures and The average MLV radii were estimated using $^2$H NMR by probing the diffusion and anisotropy of $D_2O$ within the bilayers of the vesicles. The NMR results show that as the polymer concentration was increased from 0 to 10 wt%, an increase in average multilamellar vesicle size from ~200 to ~500 nm was observed. This increase in calculated average MLV radius likely results from depletion flocculation induced MLV fusion.

## Introduction

Sodium linear alkylbenzene sulphonate (NaLAS) is the main surfactant constituent of laundry detergent and is the most widely used anionic surfactant in the world. It is used in emulsifiers, detergents and wetting agents. The phase behaviour of NaLAS in water has been characterised with respect to the different phases that form at different temperatures and concentrations.[1–3] For example, Richards et al.[4] and Stewart et al.[1] studied the phase behaviour of NaLAS in water. Both studies showed that at low NaLAS concentrations, a single micellar ($L_1$) phase was present. There was a central region where the liquid crystal ($L_\alpha$) lamellar phases coexisted with the micellar phase, and finally at high concentrations, a crystalline phase was observed. Richards[4] first observed the phenomenon of lateral phase separation in this central 2-phase region, describing a single lamellar phase at low temperatures and a second swollen lamellar phase with a higher bilayer spacing was observed at high temperatures. However, Stewart observed three lamellar phases in this high temperature region and two lamellar phases in the low temperature region.[1,5]

In liquid and powder detergent products, NaLAS usually coexists with polymers. The $d$-spacing of the lamellar phase is used to characterise the length scale of the phase which

is comparable in size to the length scale of water-soluble polymers, namely polycarboxylate polymers.[6,7] These polymers are fundamental in the formulation of powdered detergents for the following reasons: (i) to disperse salt crystals such as calcium carbonate, consequently preventing them from growing into larger crystals which can deposit on fabric and cause them to grey.;[8] (ii) to bind to calcium and magnesium ions which are present in hard water;[8] and iii) to modify the slurry viscosity in order to improve the ease of slurry processing.[8] Understanding the interaction of polymers with surfactants is imperative in washing powder formulation to achieve a desirable product quality; the formulation directly influences the powder structure and hence the performance of these detergent products.[9]

There are two colloidal structures the lamellar phase can self-assemble into: multilamellar vesicles and lamellar sheets. The formation of these micro-structures is sensitive to various conditions such as the shear history of the surfactant mixture, temperature and heating/cooling rates.[1] Due to the turbid nature of the mixtures containing multilamellar vesicles dispersed in the isotropic phase, the techniques available to measure the sizes of the vesicles are very limited. Dynamic light scattering (DLS) is not usually an option for characterising the vesicle sizes of NaLAS-water systems at high concentrations due to the multiple scattering resulting from the sample turbidity. Small angle x-ray scattering (SAXS) and DLS are unsuitable for characterising the vesicle sizes in this system due to the high fluid viscosity and vesicle sizes that are way beyond the limit of detection by DLS and SAXS. Laser diffraction is often considered for the sizing of particles in solution. This technique is unsuitable for NaLAS systems - this is because it requires the dilution of the surfactant. This dilution can completely alter the phase behaviour.

A final option that is often considered for the visualisation and size determination of these vesicles is cryo-EM (both TEM and SEM). This a technique extensively used to image the microstructure of surfactant systems. However, this again proves unsuitable for this system. Khodaparast at al.,[10] observed the formation of multilamellar vesicles upon cooling of dilute surfactant concentrations by SAXS. At lower surfactant concentrations, no lamellar

phase was observed at higher tempeatures (only a single micellar phase). However, upon rapid cooling of this micellar dispersion, MLVs rapidly self-assembled - the size of these vesicles were dependent upon the cooling rate. SAXS was used in this system because the low concentrations of NaLAS explored meant the ionic concentration was low. In cryo-EM, cooling is usually fast, but not instant. Therefore, the structure locked in is not necessarily representative of the system at the temperature being considered. This therefore makes cryo-EM imaging unsuitable for this system.

Due to the difficulty in determining the vesicle size, to date, no quantitative technique has been used to measure the vesicle size in NaLAS surfactant systems. This paper will present the first calculations of the average MLV vesicle radius in NaLAS-water systems, as well as the changes in average MLV size observed upon the addition of a polycarboxylate polymer.

This work will build on a method of calculating the radius of multilamellar vesicles introduced by Medronho[11] using $^2$H NMR measurements. The assumption of the slow exchange of water molecules between adjacent layers implies that the $^2$H NMR line shape is simply given by a sum of Lorentzians if the condition of motional narrowing is also fulfilled. The classical two-step model for the NMR relaxation in structured fluids allows the calculation of MLV radius.[5,12]

Furthermore, this paper will also describe the phase behaviour of a NaLAS-polycarboxylate polymer system using microscopy and phase differentiation by centrifugation. This will be achieved by presenting a surfactant-polymer phase diagram, and corroborating the NMR observations used to calculate the MLV radius with the phase behaviour obervations in order to gain a comprehensive understanding of the surfactant-polymer interactions.

$^2$**H NMR for structural analysis.** $^2$H NMR is an effective tool to characterise the phase behaviour of lyotropic surfactant mesophases as the line shape can be used to identify the presence of different lyotropic mesophases. The technique probes the motion averaged electric quadrupole couplings between the deuterium nuclei which have a spin of 1 and the

electric fields in the direct vicinity of the deuterium nuclei. Lamellar sheets are anisotropic and the $D_2O$ molecules are constricted between the bilayers, which is manifested as a doublet on $^2H$ NMR spectra. Often, two pairs of these doublets can be observed on NMR spectra: one pair corresponding to the sheets aligned parallel to the magnetic field and the other pair corresponding to the sheets aligned perpendicular to the sheets.[13] This combination of pairs in the NMR spectra is known as quadrupolar splitting. The frequency difference between the each doublet peak pair depends on the surface curvature of the interface. The lamellar structures present uniaxial symmetry and the splitting observed on the $^2H$ spectra can be described as follows:

$$\Delta\nu_{Q,90} = \frac{3}{2}\chi\overline{(\cos^2\theta - 1)}, \tag{1}$$

where $\theta$ is the angle between the director (the symmetric axis of the phase) and the magnetic field, $\delta$ is the motionally averaged quadrupolar coupling constant for C-$^2H$ bonds and $\chi$ is the quadrupolar coupling constant for deuterium. In accordance with Equation 1, the NMR line shape depends directly upon the director distributions. This can also be simplified as:

$$\Delta\nu_{Q,90} = \frac{3}{4}|\chi S|, \tag{2}$$

where $S$ is the order parameter.[13]

Translational diffusion of water in lamellar phases is anisotropic and confined to a given bilayer. Therefore, the average multilamellar vesicle size is directly dependent upon translational diffusion of water bound within the bilayers. The water in the planar lamellar sheets have no rotational diffusion component, apart from the local anisotropic tumbling. As the curvature of the sheets increases, there is an associated rotational diffusion term and the quadrupolar splitting decreases. Eventually, as the curvature increases such that the vesicles are formed, the quadrupolar splitting transforms into a single broad peak when multilamellar vesicles are formed, which corresponds to the average of one or more quadrupolar splitting values. When sheets coexist with vesicles, both a broad peak and the quadrupolar splitting

can be observed in the NMR spectra.[13]

The line width of the central peak can be related to the transverse relaxation time as a result of the Heisenberg uncertainty principle.[14] This relationship is defined as:

$$\frac{1}{T_2} - \frac{1}{T_1} = \frac{9\pi^2}{40} J_{dl}(0)|S\chi|^2,$$

(3)

where $J_{dl}(0)$ is the zero-order spectral density resulting from diffusion of water over the curved bilayers. Assuming that the water is experiencing variations of director orientations by translational motion and the diffusion of this water is characterised by the rate of diffusion, $D$, the residual anisotropy remaining after partial averaging by the fast motions is quantified by an order parameter, $S$, and $\chi$ is the quadrupolar coupling constant for C-D. Then, the the following can be inferred in terms of the multilamellar vesicle radius, $R$:[13]

$$J_{dl}(0) = \frac{R^2}{3D}.$$

(4)

The longitudinal ($T_1$) relaxation time for heavy water is much larger than the transverse ($T_2$) relaxation time for $^2$H NMR, $\frac{1}{T_1}$ is negligible compared to $\frac{1}{T_2}$, therefore, a combination of Equations 2, 3 and 4 gives:

$$\frac{1}{T_2} = \frac{2\Delta\nu_{Q,90}^2 R^2}{15D},$$

(5)

As a result of the Heisenberg uncertainty principle, one can define the $\frac{1}{T_2}$ relaxation in terms of the half-width at half-maximum ($\Delta\nu_{\frac{1}{2}}$) of the corresponding peak:

$$\frac{1}{T_2} = \pi\Delta\nu_{\frac{1}{2}}.$$

(6)

The isotropic peak will have a contribution of water associated with the micelles and free water in the isotropic phase, however the $T_2$ of both contributions is much larger than the $T_2$ of water confined in the MLVs, so the half-width at half maximum (HWHM) of the isotropic peak contribution will be have to be accounted for. To do this, the spectra for the surfactant

in the micellar phase is measured. For example, for 10 and 15 wt%, a single peak should be observed corresponding to the micellar phase. The HWHM of the peak measured which should remain roughly constant regardless of the surfactant concentration, and this should be subtracted from the HWHM of the higher concentration samples. The resulting HWHM value following subtraction should account solely for the water associated with the MLVs and this value can be used to calculate the MLV radius.[11]

Obtaining the $^2$H NMR spectrum for a sample can provide values of both the HWHM of the isotropic peak and the quadrupolar splitting value corresponding to that sample which can subsequently be used to determine the average multilamellar vesicle size.

## Experimental section

**Chemicals.** Commercial linear alkylbenzene sulphonic acid (HLAS) was provided by Procter and Gamble. The HLAS is composed of a number of different alkyl chain lengths and positional isomers (the benzene ring is substituted on any carbon other than the terminal carbons, see Fig. 1). It is manufactured using the Hydrogen Fluoride (HF) process, where n-Paraffins are broken down into n-mono-olefins and the n-mono-olefins are reacted with benzene in the presence of a HF catalyst to produce a linear alkylbenzene (LAB) and subsequently the LAB is sulphonated to leave HLAS. The HF results in a isomer distribution with an equal preference of each positional isomer. Other manufacturing routes produce HLAS with an uneven distribution of positional isomers.

HLAS was neutralised with analytical grade NaOH. The pH was measured and additions of NaOH/water/HLAS were made as necessary to leave a 45 wt% in water surfactant solution with a pH of 10.4. The polymer used (BASF) was provided as a stock solution of 40 wt% in water with a pH of 7, the polymer structure is depicted in Figure 1. It is a maleic-acrylic polycarboxylate polymer, where the acrylic:maleic molar ratio is 0.7:0.3. For the NMR experiments, the neutralised surfactant was oven dried for 24 hours at 90 °C for

moisture removal, yielding a concentration of 97 wt% NaLAS (as determined from mass loss measurements). This was consequently reconstituted with $D_2O$ and the polymer solution was added to yield the concentrations required for the samples. The samples were then stirred at 70 °$C$ with a magnetic stirrer for one hour and placed in NMR tubes. The samples were analysed by NMR three days after initial preparation. In the case of analysis by centrifugation, SAXS or microscopy, the stock solution was not dried, and instead diluted using the stock polymer solution and water to obtain the desired sample concentrations.
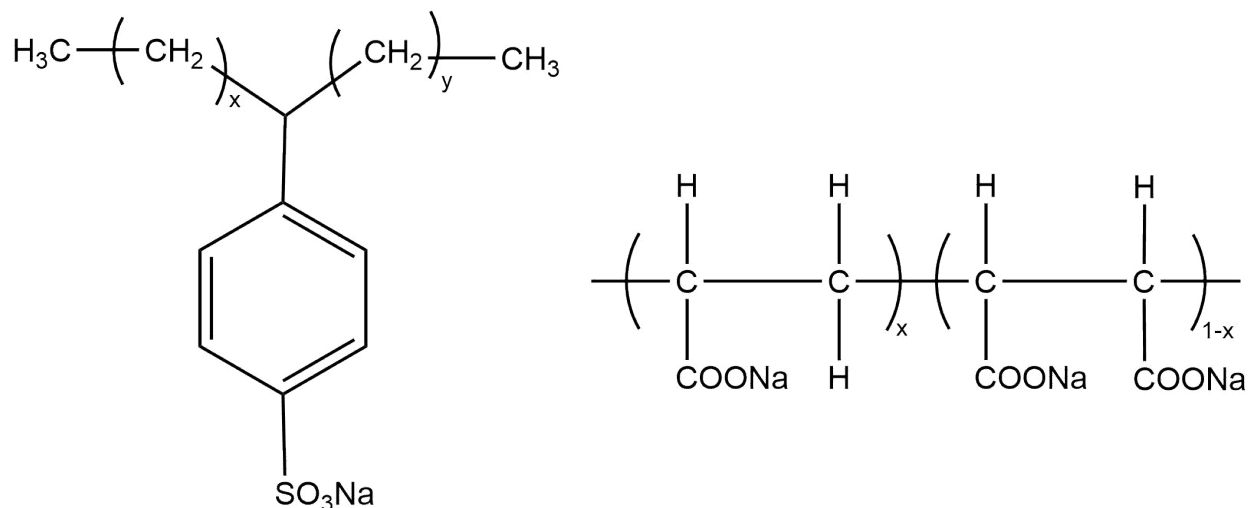


Figure 1: Structure of the surfactant used (left) and the polymer used (right).

**Centrifugation.** The difference in bulk density of the phases means that the application of a centrifugal force can allow phase differentiation by applying a centrifugal force. This phase identification technique was therefore used as one of the techniques to determine the phase diagram of the tertiary NaLAS-polymer-water system. All experiments were carried out at 50 °$C$ using the Lum GmbH Lumisizer. The centrifuge was heated to 50 °$C$ and the samples were equilibrated to the centrifuge temperature for 10 minutes before they were centrifuged at 4000 RPM for 137 minutes. The equipment contained light sensors to detect any further movement of sedimentation/creaming fronts and in all samples the separation was completed within 137 minutes. These samples were then visually analysed to observe the different phases present.

**Microscopy.** A Leica DMLP polarizing optical microscope was used to analyse samples between crossed-polarisers. All samples that were analysed were sandwiched between two cover slips and placed in a Linkam T95-PE hot stage. The samples were heated from the room temperature to $50\,^{\circ}C$ at a rate of $10\,^{\circ}C/\mathrm{min}$. The samples were left in the hot stage for 5 min before the structures were subsequently analysed. In some cases, a full-wave plate was inserted along the optical path to emphasise the birefringence. Micrographs were captured using a Nikon D7100 DSLR camera.

**$^2$H NMR spectra acquisition.** A Bruker Avance II 400-MHz-NMR was used with a $^2$H resonant frequency of 61 MHz. Each sample that was analysed was individually shimmed and left to equilibrate at 50 °C with the magnetic field for 40 minutes. The samples were analysed 3 days after sample preparation and 32 scans were carried out on each sample, a 90° p1 pulse time of 7.65 $\mu$s was used.

**Determination of the diffusion coefficient.** Pulsed field gradient (PFG) NMR can be used to determine the diffusion coefficient of the water associated with the isotropic peak. This method employs two magnetic field gradient pulses of strength $G$ and duration $\delta$, which are separated by an observation time, $\Delta$. In the case of diffusion, where molecular motion is incoherent, molecular displacements over the time scale $\Delta$ produce a distribution of phase shifts in the magnetic resonance (MR) signal, resulting in an attenuation of the MR signal. The MR signal is acquired over a range of G values and a diffusion coefficient can be calculated by a least-square fitting of the Stejskal-Tanner equation:[15]

$$I = I_0 e^{-bD}, \tag{7}$$

where

$$b = \gamma^2 G^2 \delta^2 \tau. \tag{8}$$

The symbol $\gamma$ is defined as the gyromagnetic ratio of the nucleus, $\delta$ is the duration of the gradient pulse, $\tau$ is the separation time between pulses, $D$ is the self-diffusion coefficient of

the molecule of interest (in this case $D_2O$), $I$ is the peak intensity at a given value of $G$ and $S_0$ is the intensity when $G=0$. PFG experiments were performed on a vertical wide bore 89 Bruker 400 MHz- spectrometer equipped with a 7.0 T superconducting magnet, operating at a frequency of 400 MHz. A 10 mm radiofrequency resonator was used and measurements were performed at 50 °$C$. Typical parameters used in these experiments were $\delta = 1$ ms, $\Delta = 20$ ms, with a maximum gradient, $G$max, of 12.13 G/cm. There were 16 gradient steps, so the signal was attenuated to ensure $S(G)/S(0)$ at $G$max was $\leq 0.01$.

**SAXS.** The SAXS experiments for this study were carried out in the BM28 beamline at the European Synchrotron Radiation Facility (ESRF). The equipment set-up was such that the sample to detector distance was 1.6 m and the tube was purged with Helium. A MAR CCD detector was used and silver behenate was used to calibrate the equipment as its d-spacing is well known. The data for all spectra were background subtracted using the data collected by using a Quartz capillary SAXS tube with an inner diameter of 1.5 mm, filled with deionised water. The SAXS data was collected over a range between 0.0184 and 0.308 $\text{Å}^{-1}$. The d-spacing of the Bragg peak identified with SAXS was analysed using the Bragg equation to determine the repeating d-spacing lengths:

$$d = \frac{2\pi}{q_d},\tag{9}$$

where $d$ is the d-spacing and $q_d$ is the scattering vector at which the Bragg peak occurs.

The samples were heated using a Peltier hot stage.

## Results and discussion

**Phase diagram.** Using phase differentiation by centrifugation and cross-polarised microscopy, a phase diagram for the NaLAS-polymer-water system was constructed. The phase diagram presented in Figure 2 shows the phases present between a concentration range of 0 and 35 wt% surfactant and 0 and 10 wt% polymer. Phase boundaries were identified to
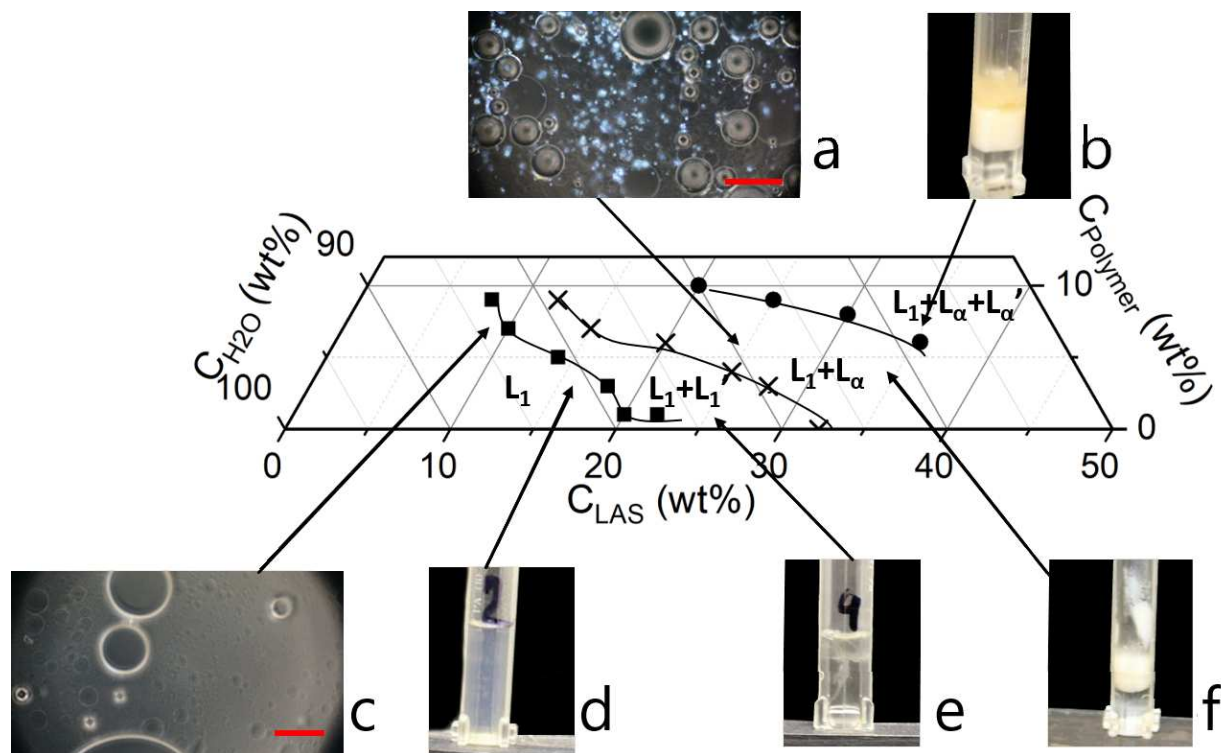
Figure 2: Ternary phase diagram of the NaLAS-polycarboxylate polymer-water system at 50 °C; the phase transitions were determined by centrifugation and cross-polarised light microscopy. $L_1$ represents the low-density isotropic phase, $L_1$' is the high density isotropic phase, $L_\alpha$ is the high density lamellar phase and $L_\alpha$' is the low density lamellar phase. The scale bar in both pictures is 25 $\mu$m. a) shows an example crossed-polarised micrograph of the 2-phase $L_1 + L_\alpha$ region, b) shows an exemplar phase differentiation by centrifugation sample vial in the 3-phase $L_1 + L_\alpha + L_\alpha$' region. The bottom phase is clear, the middle lamellar phase is creamy and opaque and the top lamellar phase is translucent and straw-coloured. c) shows a cross-polarised light micrograph of the single-phase $L_1$ region. d) shows an exemplar phase differentiation by centrifugation sample vial in the single $L_1$ region. e) shows an exemplar phase differentiation by centrifugation sample vial in the 2-phase $L_1 + L_1$' region. The bottom phase is the transparent $L_1$ phase and the top phase is the translucent $L_1$' phase. f) shows an exemplar phase differentiation by centrifugation sample vial in the 2-phase $L_1 + L_\alpha$ region. The bottom phase is the clear isotropic phase and the top phase is the cloudy lamellar phase.

the nearest +/- 1 wt% of polymer using a series of polymer solutions at a range of fixed surfactant concentrations.

The phase diagram presented in Figure 2 shows that in the absence of polymer, a single isotropic micellar phase, $L_1$, is present at concentrations lower than 35 wt% NaLAS, which is shown in Figure 2 as the $L_1$ region and the phase optically looks either like a transparent clear
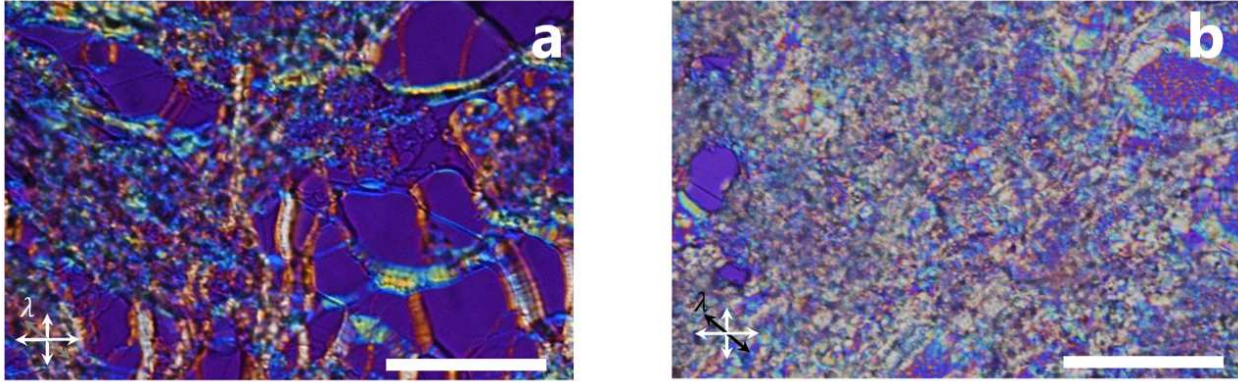
Figure 3: Cross-polarised microscopy images of the two lamellar phases viewed at 50 °C with a full wave plate to emphasise birefringence. The image on the left (a) shows the top, less dense lamellar phase ($L_\alpha$); and the image on the right (b) shows the bottom, denser lamellar phase ($L'_\alpha$)(35 wt% NaLAS, 8 wt% polymer). The scale bar in both images is 5 $\mu$m. The 2 phase lamellar region can be observed at the appropriate region in Figure 2.
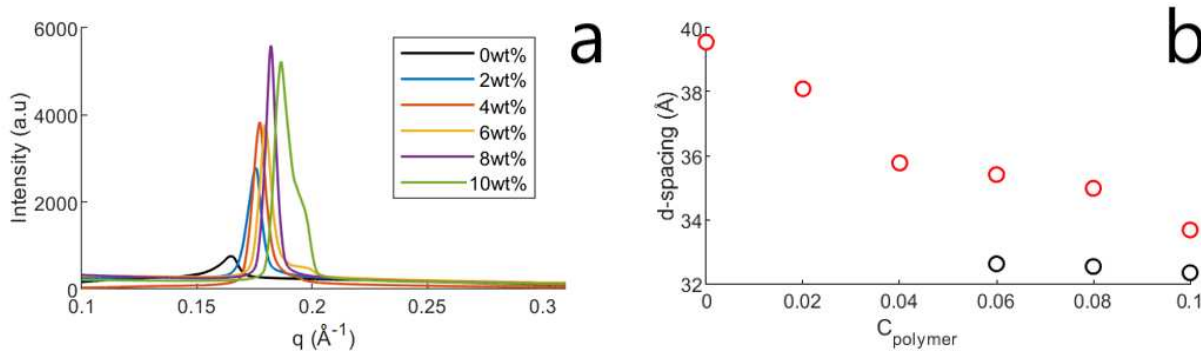


Figure 4: a) The raw intensity-q plots of the samples from which the d-spacing is determined and b) the d-spacing of the lamellar phase at a weight fraction of 0.35 in water at 50 °C NaLAS, as a function of polymer concentration determined using the Bragg equation from the SAXS experiments at 50 °C. The red circle corresponds to the d-spacing of $L_\alpha$ phase and the black circles corresponds to the d-spacing of the $L'_\alpha$ phase.

or straw colour fluid/gel. At 35 wt% NaLAS and higher, a two-phase region of coexisting micellar and lamellar phases is present, the $L_1 + L_\alpha$ region; this is in agreement with reports by Richards[4] and Stewart.[1]

In the micellar regime (which is described by the region $L_1$ on the phase diagram), as the concentration of polymer is increased, a two-phase regime is observed, the $L_1 + L'_1$ region, both phases are optically isotopic, this is depicted by $L_1 + L_1$' on the phase diagram. There is a final three phase region, $L_1 + L_\alpha + L_\alpha$' which contains an isotropic liquid as well as two

lamellar phases that differ in opacity, colour and density. These 3 phases can be observed in the centrifuge tube in Figure 2b. The bottom transparent phase is the isotropic phase, which is the most dense of all 3 phases. Above that is an opaque white lamellar phase, and above that is a yellow, translucent lamellar phase which is less dense than the opaque white lamellar phase.

The bulk phase separation observed following centrifugation (as shown in Figure 2b may result from the segregation of surfactant molecules into a high surfactant concentration phases and low surfactant concentration phases resulting from the addition of polymer. Figure 3 shows cross-polarised micrographs of the 2 lamellar phases viewed with a full wave plate - which each have the optical appearance shown in Figure 2b. Figure 3a shows the less dense lamellar phase and Figure 3b shows the denser lamellar phase. It can be seen that both lamellar phases are dispersed in an isotropic medium. However, the micrograph of the less dense phase shows fewer birefringent regions, showing the difference in microscopic packing of the lamellar phase between both phases. The $L_\alpha$'(top) phase depicts a lower density of the lamellar phase per unit area compared to the $L_\alpha$(bottom) phase. This is indicative of a difference in microscopic packing of the phases, and this can be used to explain the difference in the density of the 2 phases. Depletion flocculation of the surfactant results from the addition of polymer, if it is non-adsorbing. This depletion flocculation is observed in this system. The surfactant rich lamellar phases, upon the addition of this non-adsorbing polymer separates into two separate lamellar phase, both of which have different densities. One of the lamellar phases is polymer-rich and has a low microscopic packing of the lamellar phase, as can be observed in Figure 3a) and one is polymer poor (and has a high microscopic packing of lamellar packing, as observed in Figure 3b).[16] The tendency of non-adsorbing polymers to cause depletion flocculation in colloidal systems is well known and studied. The lamellar phase is the characterisation of the repeating adjacent lamellar layers with a defined d-spacing. These lamellar structures self-assemble into larger colloidal structures with different topologies, usually as either an array of extended parallel sheets or

the bilayers are curve and MLVs form. The topology observed depends upon the Gaussian curvature of the bilayers, $<K>$. If $<K>$ is greater than 1, MLVs form spontaneously, and if it is equal to 1, an extended planar topology is adopted. $<K>$ is directly dependent upon the saddle splay modulus, $k_b$. Systems with high ionic concentrations, such as the system studied in this paper, have a negative $k_b$ value, resulting in a negative $<K>$ value.[17]

As discussed earlier, an MLV topology is adopted by this system. In this system, depletion flocculation results when polymer chains are in regions of close approach between two neighbouring lamellar (MLV) structures. The regions between two MLVs at close approach have a low polymer concentration and there is a high polymer concentration in the bulk. This concentration gradient causes an osmotic pressure gradient, and to overcome this osmotic gradient, the 2 phases are formed.[16]
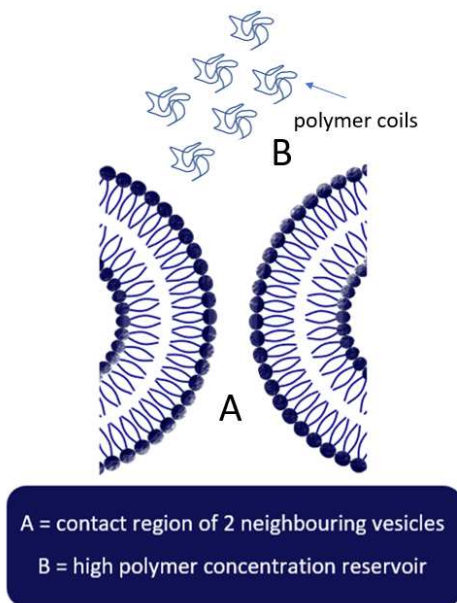


Figure 5: Schematic showing the outer bilayer of two MLVs at close approach. Region B shows the polymer-rich reservoir, resulting from the polymer being forced out from between the two multilamellar vesicles at close approach at region A.

**SAXS data**. The SAXS data presented in Figure 4 shows just a single Bragg peak at 0, 2 and 4 wt%, and two peaks at 6, 8 and 10 wt%. This indicates that the addition of polymer induces the formation of another lamellar phase, with a lower d-spacing. NaLAS has

been well documented to present multiple lamellar phases (i.e. lamellar phases of different d-spacings can co-exist in areas of the NaLAS/water phase diagram).[1,4] This SAXS data can be related to the phase diagram shown in Figure 2. In the phase diagram the $L_1 + L_\alpha + L_\alpha$' region shows two distinct lamellar phases of different densities. The same is seen with the SAXS data; as polymer is added, there is a transition from 1 lamellar phase to 2 lamellar phases. This transition is possibly the result of lateral phase separation, which has been previously been described by Richards[4] and Stewart[1] to occur in NaLAS-water system due to the inhomogeneity in chain lengths, and a segregation of these chain lengths results in the formation of lamellar phases with different d-spacings on cooling, the differences in d-spacing is to be expected, as the lamellar d-spacing of the different positional isomer varies.[18] Both Stewart and Tiddy observed separate peaks close to each other, usually manifested as a double shoulder in their SAXS data. This lateral phase separation in NaLAS has also been observed by Ockelford[19] and Ma.[18] Farschi[20] also observed this lateral phase separation phenomenon in dry NaLAS. Richards[4] observed a d-spacing of 30.6 Å for 35 wt% NaLAS in water, Stewart[1] observed a d-spacing of 33.5 Å and this study shows a d-spacing of 39.6 Å. This difference is likely due to the difference in isomeric composition of the NaLAS used in each study. The d-spacing has been shown to decrease as a result of the increasing concentration of electrolyte,[21,22] the addition of polymer seems to induce a similar effect, again likely due to the aggregation of the surfactant headgroups, but also, the polymer is charged so the addition of the polymer will increase the ionic strength of the system. The intensity of the SAXS peaks increase as a function of polymer concentration (apart from a slight decrease after 8 wt% polymer). This is because the increased concentration of the lamellar phase in each sample as the polymer is increased so there is more lamellar phase to scatter the incident X-rays.

**Phase behaviour of the 35 wt% NaLAS system, with increasing polymer concentration.** Figure 6 shows the cross-polarised micrographs of 35 wt% NaLAS in water as the concentration of the polymer was increased. The image for each sample shows Maltese
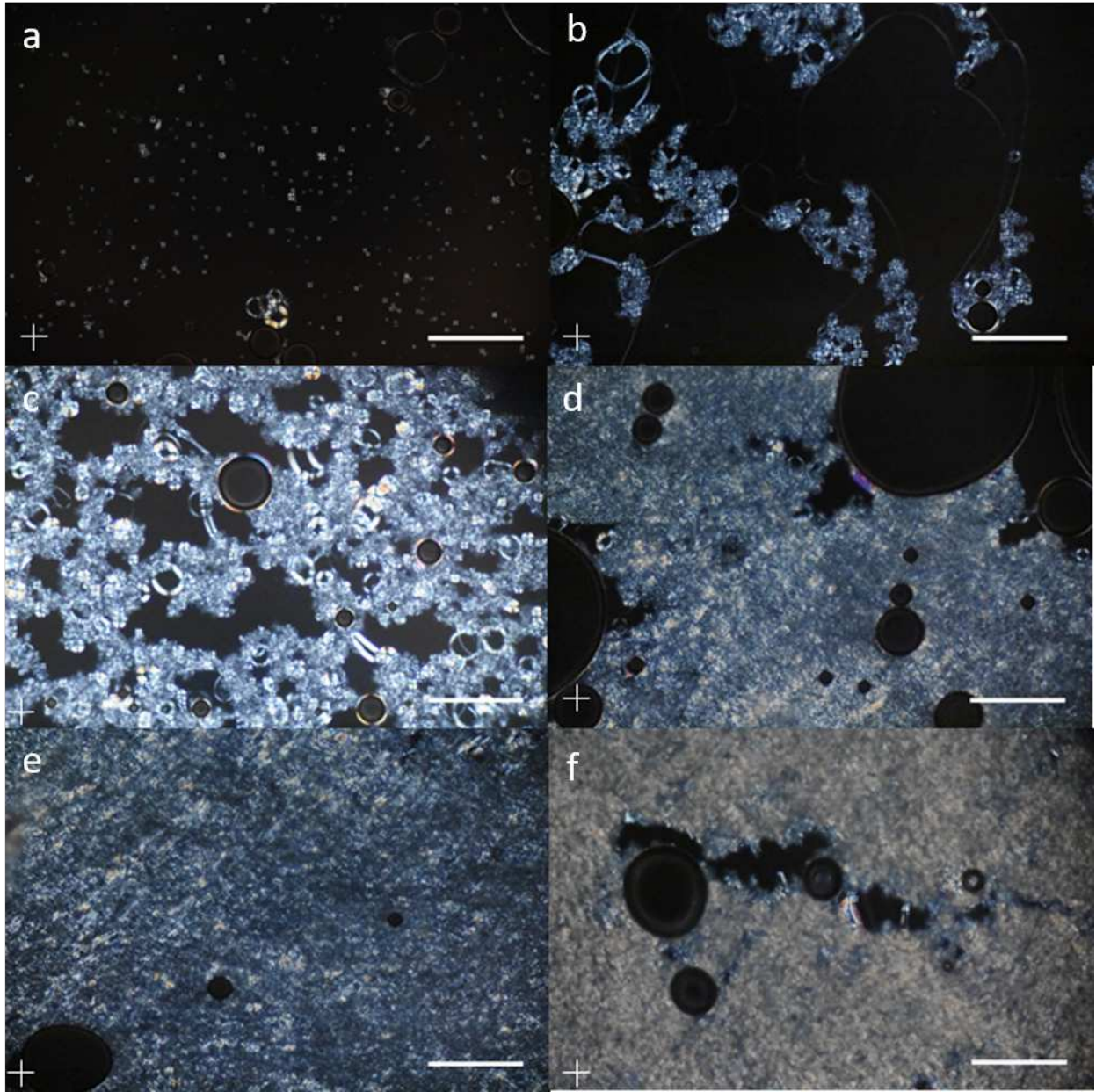
Figure 6: Cross-polarised light micrographs at 50 °C: a) 35 wt% NaLAS in $D_2O$; b) 35 wt% NaLAS, 2 wt% polymer in $D_2O$; c) 35 wt% NaLAS, 4 wt% polymer in $D_2O$; d) 35 wt% NaLAS, 6 wt% polymer in $D_2O$; e) 35 wt% NaLAS, 8 wt% polymer in $D_2O$; f) 35 wt% NaLAS, 10 wt% polymer in $D_2O$. The scale bar represents $5\mu$m.

crosses against a black background, which is indicative of multilamellar vesicles dispersed in an isotropic medium. As the concentration of polymer is increased, the density of these Maltese crosses on the micrographs is increased. This is a result of the polymer inducing the conversion of the micellar phase into the lamellar phase, perhaps due to the increase in

16

ionic strength which results from the addition of the polymer. The increase in ionic strength causes micelle aggregation by dehydrating the micelle headgroups converting - causing the micelles to aggregate and form vesicles.[21]

**Lamellar structure analysis by $^2$H NMR.** Figure 7 shows an NMR spectrum for 35 wt% NaLAS and 6 wt% in $D_2O$ at 50 °C. The spectrum was acquired after the sample in the NMR tube was equilibrated to the temperature and the magnetic field for 40 minutes. The inset (b) shows the full spectrum and the main figure (a) shows the spectrum zoomed in to enable details of the quadrupolar splitting and the central isotropic peak to be seen. Figure 8 shows the NMR for 2, 4, 6, 8 and 10 wt% polymer all with 35 wt% NaLAS in $D_2O$. Clearly, as the polymer concentration increases, the central peak broadens. Each data set shows the corresponding fit. The central isotropic peaks are fitted to the Lorentzian model and the quadrupolar peaks are fitted to an asymmetric Lorentzian function. Details of the fitting parameters are shown in the supporting information file.[23]

Figure 9 displays the variation of the quadrupolar splitting, the half-width at half-maximum (HWHM) of the Lorentzian fit of the isotropic peak, the diffusion coefficient of the isotropic peak and the calculated multilamellar vesicle radii values as a function of polymer concentration. The HWHM value shown in Figure 9 is the HWHM of the spectrum, with the HWHM for the micelle solution contribution being subtracted to leave just the MLV contribution (the NMR spectra of the micellar dispersions are shown in the supplementary information). The micelle solution contribution for 10 and 15 wt% was determined to be 3 Hz. As the concentration of polymer increases, the HWHM of the isotropic peak also decreases, implying that the corresponding $T_2$ correlation time increases. From Equation 5, it can be seen that $T_2$ is dependent upon the MLV size, diffusion coefficient and quadrupolar splitting, therefore it is difficult to determine how much $T_2$ is influenced by each individual factor.

It can be seen in Figure 9 that there is an increase in quadrupolar splitting from 2 to 4 wt% polymer, then a gradual decrease as a function of concentration. This shows an average
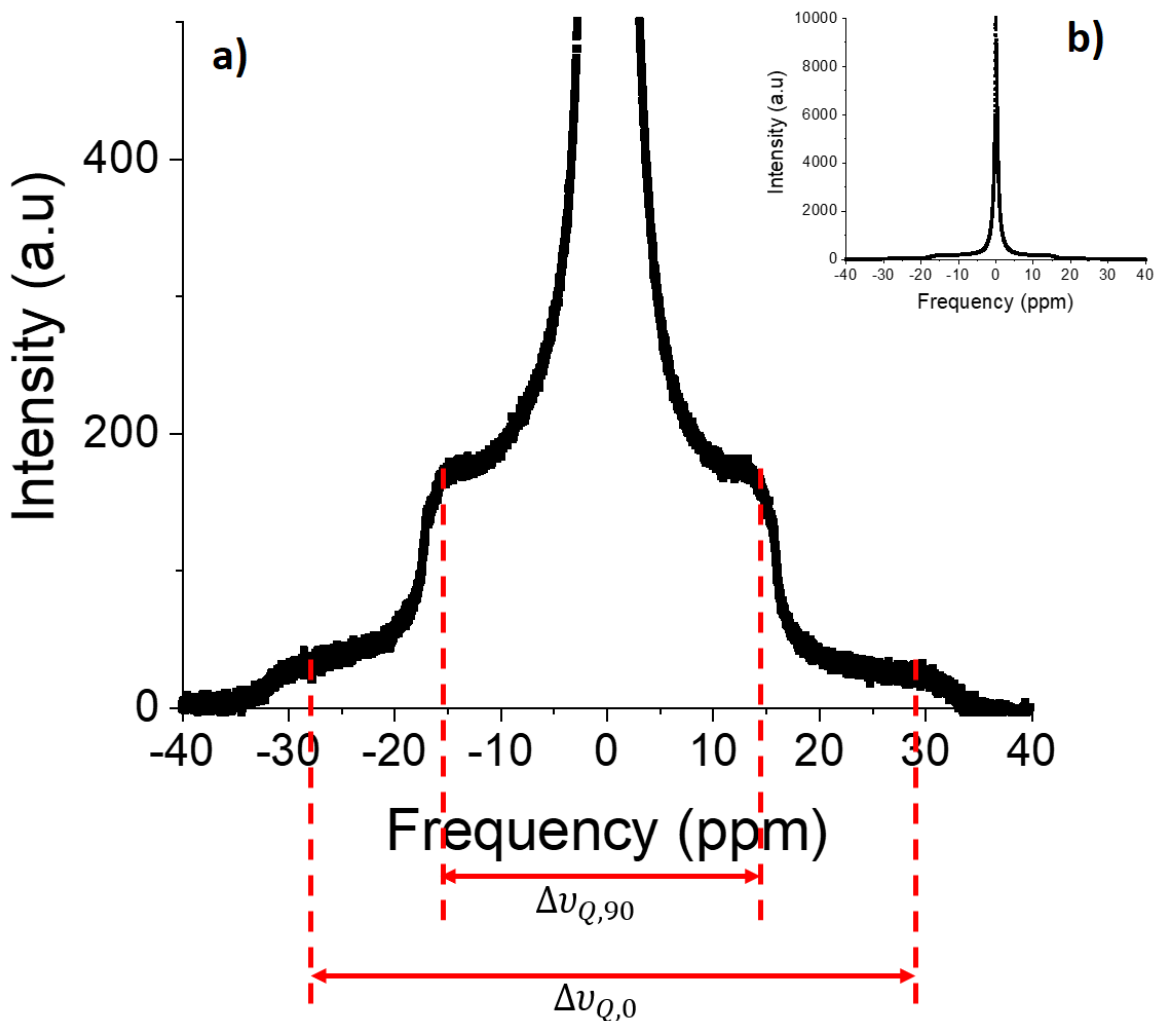
Figure 7: NMR spectrum of 35 wt% NaLAS and 6 wt % polymer at 50°C, after the sample in the NMR tubes was equilibrated with the magnetic field for 40 minutes. The inset (b) shows the spectra zoomed out and the main figure (a) shows the spectra zoomed in to show details of the quadrupolar splitting and the central isotropic peak. This frequency is presented in ppm, this could easily be converted to Hz by multiplying by the instrument frequency, 61.43 Hz in this case.

overall increase in order and subsequently a decrease, in accordance with Equation 2. Once the parameters are fitted to the vesicle size model, an increase in average vesicle size can be seen as a function of polymer concentration. Although the sizes of the vesicles are sensitive to many parameters, such as the application of shear during sample preparation and time taken between sample preparation and NMR analysis of the sample, the experiments were
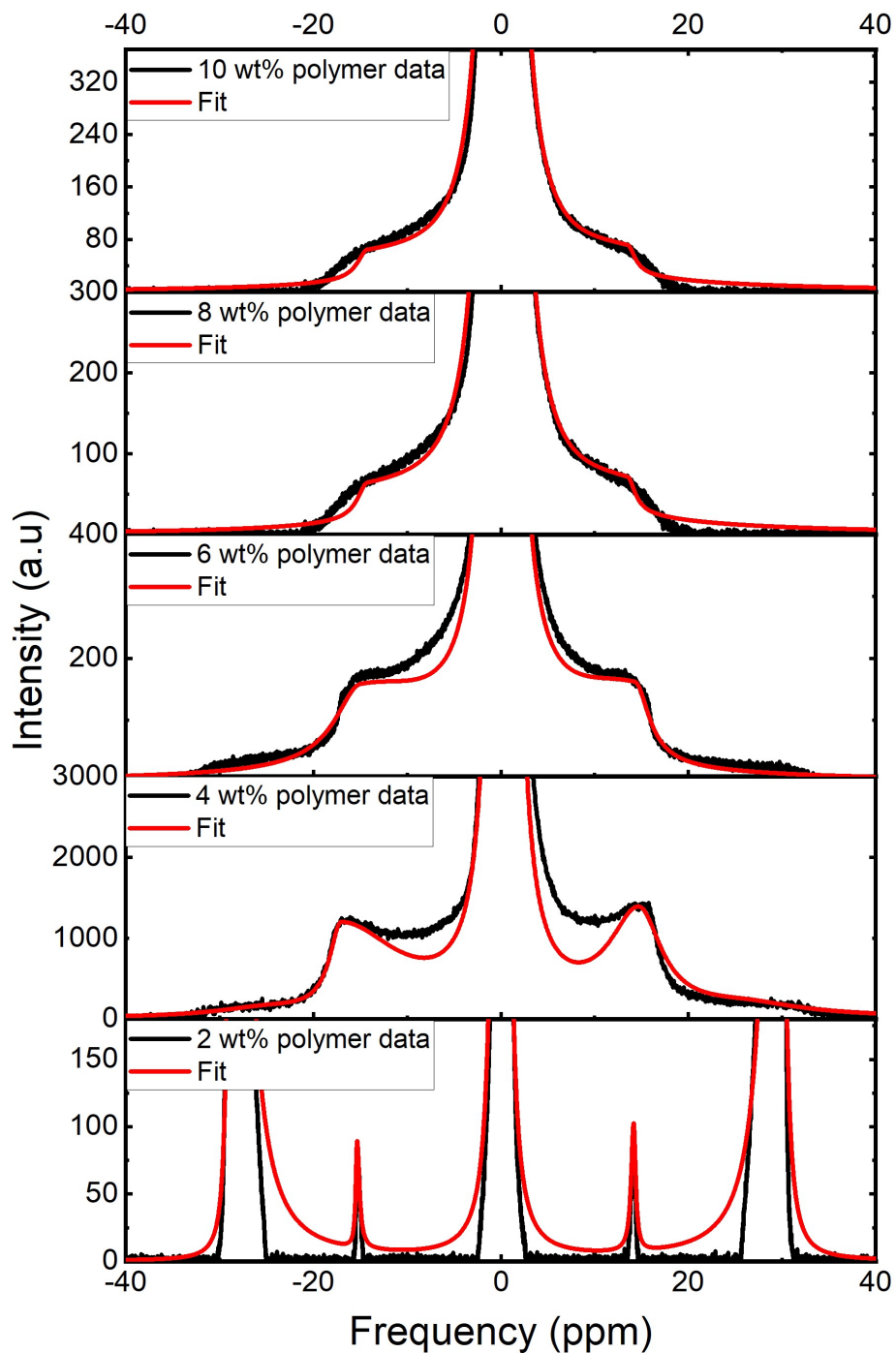
Figure 8: NMR spectrum of 35 wt% NaLAS and 2, 4, 6, 8 and 10 wt % polymer at 50°C, after the sample in the NMR tubes was left in the machine at 50 °C for 40 minutes so the temperature of the sample can reach equilibrium with the NMR machine. The data is presented on a semi-logarithmic scale to show the fitting clearly. Further fitting details are shown in the supplementary information file.
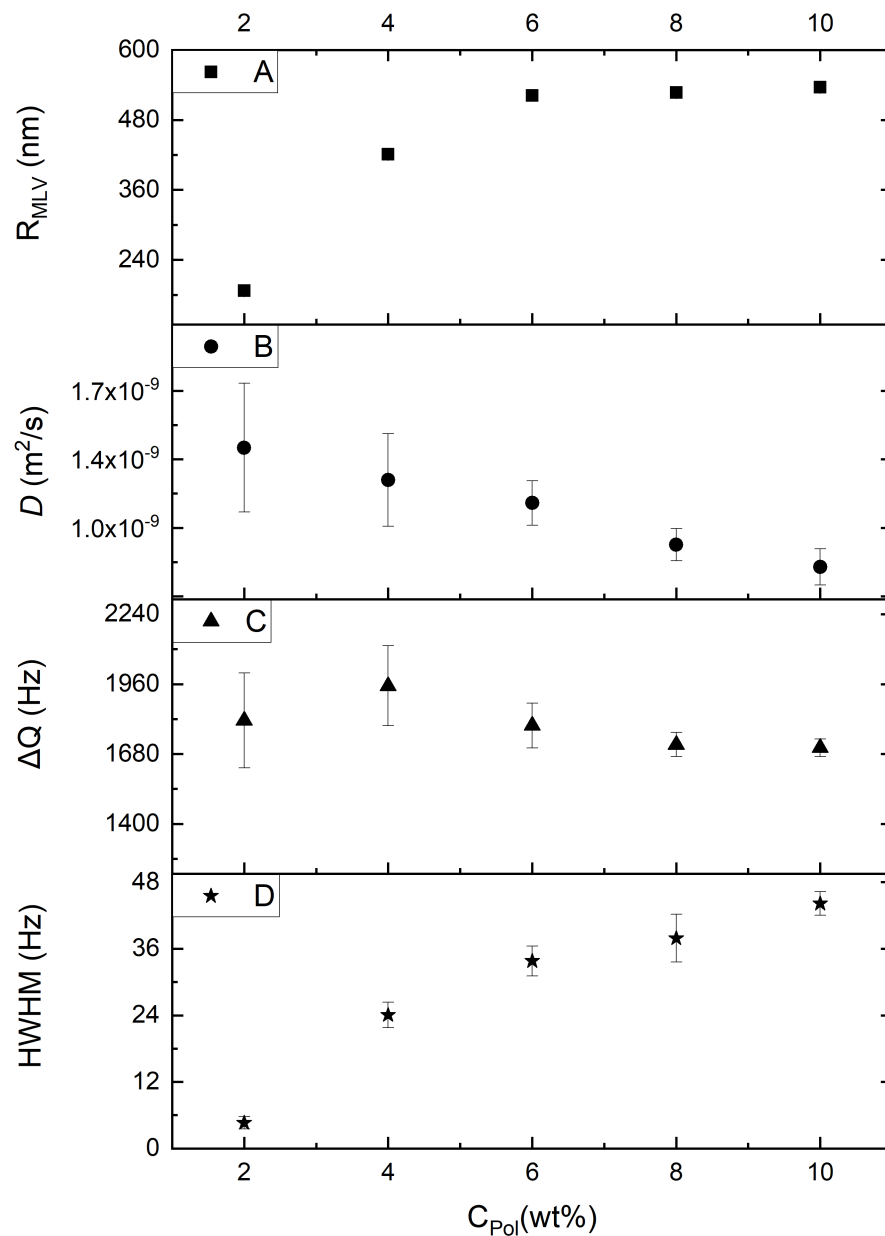
Figure 9: Data from NMR, all at 35 wt% NaLAS in water at varying polymer concentrations, at 50°C. A) shows the calculated MLV radius as a function of polymer concentration determined by using the data in graphs b to d, B) shows the variation of diffusion coefficient corresponding to the isotropic peak as a function of polymer concentration, C) shows the variation of the quadrupolar splitting as a function of polymer concentration, and D) shows the variation of the half width at half maximum of the lorentian fits of the central isotropic peaks. The error bars are based on standard deviations of repeated data sets.

repeated and the trend in size was consistently seen, as displayed in the error bars in Figure 9.

Furthermore, Figure 9 also shows a decrease in the diffusion coefficient corresponding to the isotropic peak as a function of polymer concentration. Poulos[24] stated that for NaLAS, the bilayer thickness is approximately 18-22 Å, so subtracting that from the d-spacing, the water thickness decreases from about 19 at 2 wt% polymer to 14 Å and 10 wt% polymer. Farimani and Aluru[25] have reported that when considering water confined in channels, as the channel thickness increases from 10 to 25 Å, the diffusion coefficient increases, but as the channel thickness increases from 25 to 50 Å, the diffusion coefficient decreases. So, comparing the trend in d-spacing to the study by Farimani and Aluru,[25] and relating this to the change in diffusion coefficient, an increase in diffusion coefficient would be expected. However, the NaLAS-polymer-water system is significantly more complicated than water confined in between a channel. There are additional surface, Van der Waals and electrostatic interactions which may come into effect when considering the diffusion of the water in the bilayer.

A second factor that needs to be considered when interpreting the diffusion coefficient data was that the diffusion coefficient measured represents all isotropic water present. Often, different populations of water in a sample that have different diffusion coefficients can be fitted using the Stejskal-Tanner Equation (Equations 7 and 8) as a sum of exponentials for each population. An attempt was made to fit the diffusion coefficient data to multiple exponentials when determining $D$ using the Stejskal-Tanner equation, however, the best fit was observed from a single fit. Now, despite this, there is likely to be multiple contributions to the diffusion coefficient. Both the bulk water, and the water confined in the bilayers of the vesicles. the diffusion of the water associated with the lamellar sheets is not represented by the isotropic peak. As the polymer concentration increases, the density of the lamellar phase increases. Therefore, the contribution of the water from the interlamellar water will be higher at higher polymer concentrations than at lower concentrations. When considering that the bulk diffusion coefficient of water is significantly higher than the diffusion coefficient

of water in the bilayers, it can be seen that the weighted average of these diffusion coefficients will be more influenced by the inter-bilayer water at higher polymer concentrations. So, if all factors remained the same, but all that changed was the ratio of the water between the MLV bilayers and water in the bulk, as the ratio increased, as occurs with a polymer concentration increase, the diffusion coefficient would increase. So, this change in ratio may also be contribution to the decrease in diffusion coefficient.

**Evidence that the observed behaviour is due to the depleting effect of the polymer.** The presence of the polymer in the micellar solution (where the micelles and polymer have the same charge) results in negative adsorption (desorption) of the polymer on the surface of the micelle. This negative adsorption causes an osmotic pressure potential and once the micelles are in close proximity to one another, they aggregate. This is an appropriate prediction, as both the micelle and the polymer will both be negatively charged, so it is reasonable to predict that a mixture of both components could result in depletion flocculation. This phenomenon results in phase separation with a surfactant-micelle-rich region and a polymer-rich region, as seen in the phase diagram as the $L_1 + L_1'$ region.

A lot of the behaviour seen within the phase diagram, such as the macroscopic phase separation of the lamellar phase, the phase separation of the isotropic phase and the decrease in MLV size as a function of polymer concentration, implies that the addition of polycarboxylate polymer causes depletion flocculation. This behaviour has been observed in various polymer-surfactant systems, such as PVP polymer/SDS surfactant mixtures[26] and Triton X-405 surfactant/D-glucopyranose polymer mixtures.[27] A possible mechanism behind the increase in the average vesicle size as a function of polymer concentration can be described by the depletion flocculation phenomenon, as explained by Leneveu[28] and van de Pas.[6,29] In a system containing multilamellar vesicles, the addition of a polymer which has a radius of gyration equal to or greater than that the length of the interlamellar water thickness, it will be energetically unfavourable for the polymer chains to remain confined between the lamellar layers. Hence, the polymer chains are expelled out of the vesicles. This then results

in an osmotic pressure gradient and, therefore, an increase in the Gibbs free energy of the system. Therefore, to reduce the Gibbs free energy of the system, there is a compression of the vesicles caused by reducing the interlamellar water layer thickness as the water is forced out of the vesicle, this decrease in water layer thickness may perhaps be the cause of the decrease in d-spacing as a function of polymer concentration as the water follows the osmotic pressure gradient. To overcome this osmotic pressure difference, the vesicles fuse together. The mechanism behind multilamellar vesicle fusion is not yet well understood, however the mechanism of the formation of unilamellar vesicles (ULVs) resulting fusion due to depletion flocculation has been described by Cullis[30] and Safran.[31] MLVs are likely to follow the same mechanism as ULVs.

Consider 2 MLVs at close approach, as depicted in Figure 5, consider only the outer bilayer of the 2 MLVs. The close approach region (region A) is polymer-poor and therefore region B is polymer-rich. This causes the osmotic pressure gradient previously described. This osmotic gradient is energetically unfavourable, so the system is rearranged to minimise this energy. This osmotic gradient causes surfactant molecules from the outer monolayer in region A to migrate towards region B, i.e. it causes a Marangoni flow of the surfactant molecules, which results from surface tension gradients being induced as a result of the polymer concentration gradient (osmotic potential). So, there is an increased density of surfactant molecules in region A. This flow of surfactant molecules, therefore, reverses the surface tension gradients. However, in doing so, the outer monolayer surfactants leaving region B expose the hydrophobic chains of the surfactant monolayers remaining in region B to water, which is energetically highly unfavourable. However, this can be avoided if the inner monolayers of the two adjacent surfaces in region B fuse. This fusion is promoted by attractive interactions such as depletion or van der Waals effects, and is likely to occur if the two surfaces in region B are close enough; if not, fusion cannot occur and the outer monolayer of surfactants in region B cannot be used to reduce the number or size of low-density domains in region A. So, the vesicles fuse and increase in radius as a result of the

23

polymer addition.[31]

When viewing the cross-polarised light microscopy images of the 35 wt% NaLAS in water in Figure 6, there is a low density of birefringent texture around the micrograph for the case where there is no polymer and a low concentration of the lamellar phase, although there seems to be aggregation of the vesicles. As polymer concentration is increased, there is strong aggregation of the dispersed phase, which is perhaps indicative of depletion flocculation. However, it is also a common result of decreased electrostatic repulsive interactions which can occur as a result of increasing the ionic strength of the system. The presence of polymer results in the increase of the ionic strength of the system, so it is difficult to attribute how much each factor contributes to the aggregation because the polymer itself is charged.

# Conclusions

The influence of polycarboxylate polymer on the phase behaviour of a NaLAS-water system was investigated. A phase diagram was constructed using cross-polarised light microscopy, SAXS and centrifuge phase separation. The average radii of MLVs were also calculated using a model fitted to deuterium NMR data. At low surfactant concentrations, the addition of polycarboxylate initially led to the separation of 1 isotropic phase into two isotropic phases with different densities, this is thought to be a result of depletion flocculation. As the polycarboxylate level was further increased, a lamellar phase(s) was observed, likely due to the increased ionic strength of the system. At higher surfactant concentrations, the addition of the polycarboxylate polymer led to surfactant being salted out from the micellar phase into a lamellar phase. As the polymer level was increased further, phase separation was again observed - but this time it was the phase separation of the single lamellar phase into two lamellar phases with different d-spacings and densities. The lamellar phases were observed to adopt an MLV morphology, by both polarized light microscopy and deuterium NMR. Analysis of the NMR spectrum also enabled the average multilamellar vesicle radius to be

estimated. On the addition of the polycarboxylate polymer, the average MLV radius was observed to increase. This trend may be attributed to depletion flocculation and Marangoni flow effects, which led to MLV fusion and hence MLV growth.

# Acknowledgement

# Supporting Information

The NMR data fitted to the Lorentzian model in contained within the supporting information file.

# References

(1) Stewart, J.; Saiani, A.; Bayly, A.; Tiddy, G. The phase behaviour of lyotropic liquid crystals in linear alkylbenzene sulphonate (LAS) systems. *Colloids and Surfaces A: Physicochemical and Engineering Aspects* **2009**, *338*, 155–161.

(2) Sein, A.; Engberts, J. B. F. N.; van der Linden, E.; van de Pas, J. C. Lyotropic Phases of Dodecylbenzenesulfonates with Different Counterions in Water. *Langmuir* **1996**, *12*, 2913–2923.

(3) Rafique, A. S.; Khodaparast, S.; Poulos, A. S.; Sharratt, W. N.; Robles, E. S. J.; Cabral, J. T. Micellar structure and transformations in sodium alkylbenzenesulfonate (NaLAS) aqueous solutions: effects of concentration, temperature, and salt. *Soft Matter* **2020**, *16*, 7835–7844.

(4) Richards, C.; Tiddy, G. J. T.; Casey, S. Lateral Phase Separation Gives Multiple Lamellar Phases in a "Binary" Surfactant/Water System: The Phase Behavior of Sodium Alkyl Benzene Sulfonate/Water Mixtures. *Langmuir* **2007**, *23*, 467–474.

(5) Medronho, B.; Shafaei, S.; Szopko, R.; Miguel, M. G.; Olsson, U.; Schmidt, C. Shear-Induced Transitions between a Planar Lamellar Phase and Multilamellar Vesicles: Continuous versus Discontinuous Transformation. *Langmuir* **2008**, *24*, 6480–6486.

(6) van de Pas, J.; Buytenhek, C. The effects of free polymers on osmotic compression, depletion flocculation and fusion of lamellar liquid-crystalline droplets. *Colloids and Surfaces* **1992**, *68*, 127–139.

(7) Opgenorth, H.-J. *Detergents*; Springer Berlin Heidelberg, 1992; pp 337–350.

(8) Bertleff, W.; Neumann, P.; Baur, R.; Kiessling, D. Aspects of polymer use in detergents. *Journal of Surfactants and Detergents* **1998**, *1*, 419–424.

(9) Goddard, E. D. Polymer/surfactant interaction-Its relevance to detergent systems. *Journal of the American Oil Chemists Society* **1994**, *71*, 1–16.

(10) Khodaparast, S.; Sharratt, W.; Wang, H.; Robles, E. S.; Dalgliesh, R.; Cabral, J. T. Spontaneous formation of multilamellar vesicles from aqueous micellar solutions of sodium linear alkylbenzene sulfonate (NaLAS). *Journal of Colloid and Interface Science* **2019**, *546*, 221–230.

(11) Medronho, B.; Schmidt, C.; Olsson, U.; Miguel, M. G. Size Determination of Shear-Induced Multilamellar Vesicles by Rheo-NMR Spectroscopy. *Langmuir* **2010**, *26*, 1477–1481.

(12) Schäfer, H.; Mädler, B.; Sternin, E. Determination of Orientational Order Parameters from 2H NMR Spectra of Magnetically Partially Oriented Lipid Bilayers. *Biophysical Journal* **1998**, *74*, 1007–1014.

(13) Ferreira, T. M.; Bernin, D.; Topgaard, D. NMR Studies of Nonionic Surfactants. *Annual Reports on NMR Spectroscopy* **2013**, 73–127.

(14) Szántay, C. NMR and the uncertainty principle: How to and how not to interpret homogeneous line broadening and pulse nonselectivity. III. Uncertainty? *Concepts in Magnetic Resonance Part A* **2008**, *32A*, 302–325.

(15) Ghi, P. Y.; Hill, D. J. T.; Whittaker, A. K. PFG-NMR Measurements of the Self-Diffusion Coefficients of Water in Equilibrium Poly(HEMA- *co* -THFMA) Hydrogels. *Biomacromolecules* **2002**, *3*, 554–559.

(16) Kalwarczyk, E.; Gołoś, M.; Hołyst, R.; Fiałkowski, M. Polymer-induced ordering and phase separation in ionic surfactants. *Journal of Colloid and Interface Science* **2010**, *342*, 93–102.

(17) Le, T.; Olsson, U.; Mortensen, K. Topological transformation of a surfactant bilayer. *Physica B: Condensed Matter* **2000**, *276-278*, 379–380.

(18) Ma, J.-G.; Boyd, B. J.; Drummond, C. J. Positional Isomers of Linear Sodium Dodecyl Benzene Sulfonate: Solubility, Self-Assembly, and Air/Water Interfacial Activity. *Langmuir* **2006**, *22*, 8646–8654.

(19) Ockelford, J.; Timimi, B. A.; Narayan, K. S.; Tiddy, G. J. T. An upper critical point in a lamellar liquid crystalline phase. *The Journal of Physical Chemistry* **1993**, *97*, 6767–6769.

(20) Farshchi, A.; Hassanpour, A.; Bayly, A. E. The structure of spray-dried detergent powders. *Powder Technology* **2019**, *355*, 738–754.

(21) Stewart, J. A.; Saiani, A.; Bayly, A.; Tiddy, G. J. T. Phase Behavior of Lyotropic Liquid Crystals in Linear Alkylbenzene Sulphonate (LAS) Systems in the Presence of Dilute

and Concentrated Electrolyte. *Journal of Dispersion Science and Technology* **2011**, *32*, 1700–1710.

(22) Sein, A.; Engberts, J. B. F. N.; van der Linden, E.; van de Pas, J. C. Salt-induced transition from a micellar to a lamellar liquid crystalline phase in dilute mixtures of anionic and nonionic surfactants in aqueous solution. *Langmuir* **1993**, *9*, 1714 to 1720.

(23) Stancik, A. L.; Brauns, E. B. A simple asymmetric lineshape for fitting infrared absorption spectra. *Vibrational Spectroscopy* **2008**, *47*, 66–69.

(24) Poulos, A. S.; Nania, M.; Lapham, P.; Miller, R. M.; Smith, A. J.; Tantawy, H.; Caragay, J.; Gummel, J.; Ces, O.; Robles, E. S. J.; Cabral, J. T. Microfluidic SAXS Study of Lamellar and Multilamellar Vesicle Phases of Linear Sodium Alkylbenzenesulfonate Surfactant with Intrinsic Isomeric Distribution. *Langmuir* **2016**, *32*, 5852–5861.

(25) Farimani, A. B.; Aluru, N. R. Spatial Diffusion of Water in Carbon Nanotubes: From Fickian to Ballistic Motion. *The Journal of Physical Chemistry B* **2011**, *115*, 12145–12149.

(26) Gargallo, L.; Dadić, D.; Martínez-Piña, F. Phase separation behaviour of polymers in water. Temperature and surfactant effect. *European Polymer Journal* **1997**, *33*, 1767–1769.

(27) Patel, P. D.; Russel, W. B. An experimental study of aqueous suspensions containing dissolved polymer. A. Phase separation. *Journal of Colloid And Interface Science* **1989**, *131*, 192–200.

(28) Leneveu, D. M.; Rand, R. P.; Pargesian, V. A. Measurement of forces between lecithin bilayers. *Nature* **1976**, *259*, 601–603.

(29) Evans, E.; Needham, D. Attraction between Lipid Bilayer Membranes in Concentrated

Solutions of Nonadsorbing Polymers: Comparison of Mean-Field Theory with Measurements of Adhesion Energy. *Macromolecules* **1988**, *21*, 1822–1831.

(30) Cullis, P. R.; Hope, M. J. Effects of fusogenic agent on membrane structure of erythrocyte ghosts and the mechanism of membrane fusion. *Nature* **1978**, *271*, 672–674.

(31) Safran, S.; Kuhl, T.; Israelachvili, J. Polymer-Induced Membrane Contraction, Phase Separation, and Fusion via Marangoni Flow. *Biophysical Journal* **2001**, *81*, 659–666.